Archives of Biochemistry and Biophysics 742 (2023) 109638

Contents lists available at ScienceDirect

Archives of Biochemistry and Biophysics

journal homepage: www.elsevier.com/locate/yabbi

The free-living flagellate *Paratrimastix pyriformis* uses a distinct mitochondrial carrier to balance adenine nucleotide pools

Justyna Zítek [a,1], Martin S. King [b,1], Priscila Peña-Diaz [a], Eva Pyrihová [b,c], Alannah C. King [b], Edmund R.S. Kunji [b,**], Vladimír Hampl [a,*]

[a] Charles University, Faculty of Science, Department of Parasitology, BIOCEV, Vestec, 252 50, Czech Republic
[b] Medical Research Council Mitochondrial Biology Unit, The Keith Peters Building, Cambridge Biomedical Campus, Hills Road, Cambridge, CB2 0XY, United Kingdom
[c] University of Stavanger, Department of Chemistry, Bioscience, And Environmental Engineering, Richard Johnsens Gate 4, N-4021, Stavanger, Norway

ARTICLE INFO

Handling Editor: Dr H Forman

Keywords:
Mitochondrion-related organelle
Mitochondrial carrier
Nucleoside/nucleotide transport
Paratrimastix pyriformis

ABSTRACT

Paratrimastix pyriformis is a free-living flagellate thriving in low-oxygen freshwater sediments. It belongs to the group Metamonada along with human parasites, such as *Giardia* and *Trichomonas*. Like other metamonads, *P. pyriformis* has a mitochondrion-related organelle (MRO) which in this protist is primarily involved in one-carbon folate metabolism. The MRO contains four members of the solute carrier family 25 (SLC25) responsible for the exchange of metabolites across the mitochondrial inner membrane. Here, we characterise the function of the adenine nucleotide carrier PpMC1 by thermostability shift and transport assays. We show that it transports ATP, ADP and, to a lesser extent, AMP, but not phosphate. The carrier is distinct in function and origin from both ADP/ATP carriers and ATP-Mg/phosphate carriers, and it most likely represents a distinct class of adenine nucleotide carriers.

1. Introduction

In aerobic mitochondria, ATP is synthesised by oxidative phosphorylation and transported to the cytosol in exchange for ADP to supply energy-requiring cellular processes [1]. In organisms that thrive in low-oxygen environments, these organelles are modified to various types of mitochondrion-related organelles (MRO), in which ATP is synthesised by substrate-level phosphorylation (hydrogenosomes) or not at all (mitosomes) [2]. As the import of proteins into mitochondria and MROs is driven by ATP [3], all types of mitochondria, including mitosomes, require an adenine nucleotide transporter to exchange ADP and ATP. The transport of metabolites across the impermeable mitochondrial inner membrane is mediated primarily by proteins of the solute carrier family 25 (SLC25) [4]. The number of SLC25 proteins is organism-dependent and tends to be lower in organisms that possess MROs: the human genome encodes 53 mitochondrial carriers [5]; eight putative carriers were found in mitosomes of *Cryptosporidium parvum* [6], and only one in *Antonospora locustae* [7].

SLC25 proteins share common features that can be identified on the sequence level. The proteins contain three homologous domains, each of approximately 100 amino acids [8], arranged three-fold pseudo-symmetrically around a central substrate-binding site. Each domain consists of an odd-numbered transmembrane helix (H1, H3 or H5), a loop with a short matrix helix (h12, h34 or h56) lying parallel to the plane of the membrane, and an even-numbered transmembrane helix (H2, H4 or H6) [9]. During transport, mitochondrial carriers cycle between two conformations, the cytoplasmic- and matrix-open states, thereby alternating accessibility of a central binding site to both sides of the inner membrane [10]. On the matrix side of each odd-numbered helix, a highly conserved motif [PS]x[DE]xx[KR] is present, the charged residues of which form a matrix salt bridge network in the cytoplasmic-open state [9,11,12]. These salt bridge residues can be braced by glutamine residues, which provide additional inter-domain interactions that stabilise the network [12]. In the matrix-open state, the even-numbered transmembrane

Abbreviations: PpMC1, distinct ADP/ATP carrier from *Paratrimastix pyriformis*; HsAAC1, ADP/ATP carrier from *Homo sapiens*; BtAAC, ADP/ATP carrier from *Bos taurus*; TtAac, ADP/ATP carrier from *Thermothelomyces thermophila*; ScAac2, ADP/ATP carrier from *Saccharomyces cerevisiae*; TgHMP31, distinct ADP/ATP carrier from *Trichomonas gallinae*; BKA, bongkrekic acid; CATR, carboxyatractyloside; Tm, apparent melting temperature.

* Corresponding author.
** Corresponding author.
E-mail addresses: ek@mrc-mbu.cam.ac.uk (E.R.S. Kunji), vladimir.hampl@natur.cuni.cz (V. Hampl).
[1] These authors contributed equally to this work.

https://doi.org/10.1016/j.abb.2023.109638
Received 7 April 2023; Received in revised form 12 May 2023; Accepted 13 May 2023
Available online 14 May 2023

helices come together towards the cytoplasmic side of the membrane, enabling the charged residues of the [YF][DE]xx[KR] motif to interact [13,14]. The tyrosine residues of the motif provide additional inter-domain hydrogen bonds to the negatively charged residues, bracing the network [15].

The ADP/ATP carriers (AAC) and ATP-Mg/phosphate carriers (APC, SCaMC) are responsible for the majority of adenine nucleotide exchange in mitochondria. AAC display strict substrate specificity and facilitate the equimolar exchange of cytosolic ADP for mitochondrial ATP produced by ATP synthase [16,17]. The mitochondrial ADP/ATP carrier is the best-studied protein of the SLC25 family, and is widespread throughout the eukaryotic tree, present also in organisms with MRO [6,18,19]. Atomic resolution structures of the AAC have been determined in the cytoplasmic-open state, inhibited with carboxyatractyloside (CATR) [9,12], and in the matrix-open state, inhibited with bongkrekic acid (BKA) [15]. Mitochondrial ATP-Mg/Pi carriers carry out the electroneutral antiport of ATP-Mg and phosphate, and, therefore, can change the mitochondrial adenine nucleotide pool [20]. Atypically for members of the family, they consist of three domains: an N-terminal calcium-regulatory domain with four EF-hands, an amphipathic helix, and a C-terminal carrier domain, which transports substrates [20,21]. In the presence of calcium, the amphipathic helix binds to the regulatory domain, whereas in its absence it binds to the carrier domain, inhibiting transport [20]. Compared to AAC, APC displays a broader substrate specificity (ATP, ADP, AMP, their deoxy-variants, ATP-Mg, phosphate, and pyrophosphate), yet its affinity to ATP is 10 to 100-fold lower than that of AAC [20,22–24]. It has been speculated that APC evolved from AAC after fusion with a calmodulin-like protein [21], however carriers that lost these additional domains have also been reported [18,25].

Putative ADP/ATP carriers have been investigated in the MRO of three parasitic protists (metamonad *Trichomonas gallinae* [26], microsporidium *Antonospora locustae* [7], amoebozoan *Entamoeba histolytica* [27]), which are distinct from canonical AAC. Their biochemical properties differ from those of archetypal AAC, as they transport AMP in addition to ADP and ATP. The *Entamoeba histolytica* carrier has even broader specificity, exchanging ATP 3′-phosphoadenosine 5′-phosphosulfate (PAPS) as well [28]. Moreover, the amino acids responsible for binding specific inhibitors of AAC in these species are not well-conserved, thus these proteins are not inhibited by either BKA or CATR [7,26,27].

Paratrimastix pyriformis is a free-living, freshwater flagellate that, similarly to *Trichomonas gallinae,* belongs to the Metamonada group [29]. Its MRO has been characterised by spatial proteomics, revealing that the organelle is not involved in Fe–S cluster synthesis [30], a common function of mitochondria and their reduced forms [31]. Yet, *P. pyriformis* MRO is essential to produce formate and folate derivates, which further supplies cytosolic one-carbon folate metabolism and the methionine cycle [30,32]. The organelle has four proteins of the SLC25 family to mediate the exchange of approximately a dozen compounds involved in the organellar metabolism, including adenine nucleotides (Fig. 1). Besides protein import, the organelle requires ATP for the activation of lipoic acid and polyglutamylation of folate species. Although it produces ATP via one-carbon folate metabolism [30], the ratio between ATP production and consumption within the organelle is unknown. Due to the reduction of organelle metabolism and the low number of putative substrates, *P. pyriformis* is an interesting model to study the function of mitochondrial carriers.

Here we functionally characterise one of the four identified carriers of *P. pyriformis* and demonstrate that it transports adenine nucleotides. The carrier exhibits a combination of features distinct from both AAC and APC and the phylogenetic analysis does not place it into either of the two known classes.

2. Material and methods

2.1. Modelling of PpMC1 protein

The structural model of PpMC1 in the cytoplasmic-open state was predicted using AlphaFold [33]. The PpMC1 model in the matrix-open state based on TtAac (Protein Data Bank entry; 6GCI) was calculated using SWISS-MODEL [34]. To reveal whether the amino acids responsible for the interaction with AAC inhibitors are conserved in PpMC1,

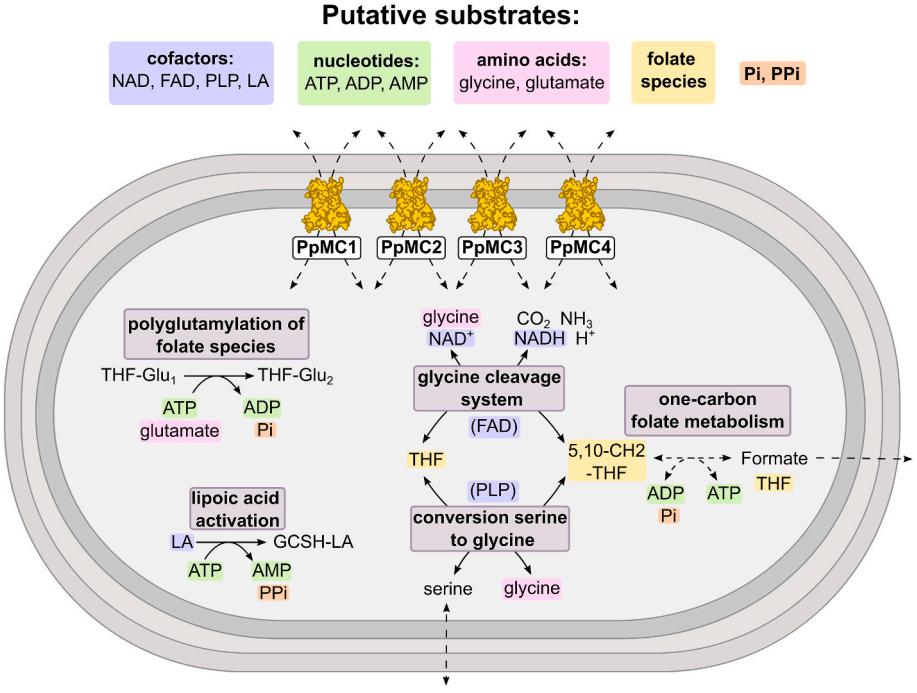

Fig. 1. Putative metabolic roles of *P. pyriformis* mitochondrial carriers.
Schematic representation of mitochondrion-related organelle metabolism and putative substrates for SLC25 proteins. PpMC1-PpMC4, *P. pyriformis* mitochondrial carriers 1–4; GCSH, glycine cleavage system H protein; PLP, phosphate pyridoxal; LA, lipoic acid; THF, tetrahydrofolate; Pi, phosphate; PPi, diphosphate.

the sequence of the protein was aligned to BtAAC inhibited by CATR (Protein Data Bank entry, 1OKC) [9] and TtAac inhibited by BKA (Protein Data Bank entry; 6GCI) [15].

2.2. Phylogenetic analysis

The dataset of 141 sequences of mitochondrial AAC, APC and distinct adenine nucleotide carriers representing a range of eukaryotic taxa was obtained by BLAST search by using human AAC1/APC1, yeast Aac2/Sal1p, *A. thaliana* AAC1/APC1, *T. vaginalis* HMP31 (homolog of distinct ADP/ATP carrier of *T. gallinae*) as a query. Additionally, the sequences of SCaMC-b, an APC lacking a regulatory domain found mainly in parasitic protists [18], the distinct ADP/ATP carrier of *E. histolytica* [27] and *A. locustae* [7] were included in the dataset. The sequences were aligned by MAFFT v7.453 [35] using the L–INS–I algorithm and a maximum of 1000 iterations. The obtained alignment was further trimmed by BMGE v1.12 [36] with an entropy threshold set to 0.7, resulting in an alignment of 254 positions. The maximum likelihood tree was generated by IQ-TREE v2.1.2 with the LG+F+R7 model suggested by ModelFinder [37]. Branch supports were generated by ultra-fast bootstrap with 10, 000 replicates. The tree with four *P. pyriformis* carriers and reference dataset (53 human carriers, 35 yeast carriers) was prepared in same way as described above. The alignment of 214 position was used to generated tree by LG + F + R6 model suggested by ModelFinder.

2.3. Protein expression in Saccharomyces cerevisiae

The gene for the putative ADP/ATP carrier from *P. pyriformis* was codon-optimised (GenScript) for expression in *Saccharomyces cerevisiae* strain W303·1B and cloned into a pYES2/CT vector (Invitrogen) under the control of an inducible galactose promoter, as previously described [38]. Transformants were selected on Sc-Ura+2% (w/v) glucose plates. A preculture of cells grown in Sc-Ura+2% (w/v) glucose was inoculated into 15 L of YPG + 0.1% (w/v) glucose medium. Cells were grown at 30 °C with shaking at 225 RPM for 20 h in flasks, induced with a final concentration of 2% (w/v) galactose, grown for further 8 h, and harvested by centrifugation (4000×*g*, 20 min, 4 °C). Crude mitochondria were prepared using a bead mill (Dyno-Mill Multilab, Willy A. Bachofen AG) by established methods [38].

2.4. Preparation of lipid for protein purification

Tetraoleoyl cardiolipin (18:1) powder was purchased from Avanti Polar Lipids. Lipids were solubilised in 10% (w/v) dodecyl maltose neopentyl glycol (Anatrace) by vortexing for 4 h to give 10 mg mL^{-1} lipid/10% (w/v) detergent stock. The stocks were stored in liquid nitrogen.

2.5. Protein purification by nickel affinity chromatography

Protein was prepared as previously described for the human ADP/ATP carrier [39]. Crude mitochondria were solubilised in 1.5% (w/v) dodecyl maltose neopentyl glycol, protease inhibitors (Roche), 40 mM imidazole and 150 mM NaCl for 1 h by rotation at 4 °C. The insoluble material was separated from the soluble fraction by centrifugation (200, 000×*g*, 45 min, 4 °C). Nickel sepharose slurry (0.5 mL, corresponding to 0.3 mL resin; GE healthcare) was added to the soluble fraction; the mixture was stirred at 4 °C for 1 h. The nickel resin was harvested by centrifugation (100×*g*, 10 min, 4 °C), transferred to a proteus 1-step batch midi spin column (Generon), and washed with 40 column volumes of buffer A (20 mM HEPES pH 7.0, 150 mM NaCl, 60 mM imidazole, 0.2 mg mL^{-1} tetraoleoyl cardiolipin/0.2% (w/v) dodecyl maltose neopentyl glycol) (100×*g*, 5 min, 4 °C); followed by 10 column volumes of buffer B (20 mM HEPES pH 7.0, 50 mM NaCl, 0.2 mg mL^{-1} tetraoleoyl cardiolipin/0.2% (w/v) dodecyl maltose neopentyl glycol) (100×*g*, 5 min, 4 °C). The nickel resin was resuspended in buffer B and incubated with 10 mM imidazole, 20 μg factor Xa protease (NEB) and 5 mM $CaCl_2$ with inversion at 10 °C overnight. The protein was eluted by centrifugation on a spin column (100×*g*, 2 min, 4 °C), and the concentration measured by spectrometry (NanoDrop Technologies) at 280 nm (PpMC1 extinction coefficient; 46,870 M^{-1} cm^{-1}, protein mass; 31.85 kDa). Imidazole and NaCl were removed using a PD-10 desalting column according to the manufacturer's instructions (GE Healthcare) at 4 °C. Protein was aliquoted, snap-frozen, and stored in liquid nitrogen.

2.6. Thermostability analysis

Protein thermostability was determined as previously described [40] using the CPM thiol-specific fluorescent probe (N-[4-(7-diethylamino-4-methyl-3-coumarinyl)phenyl] maleimide) [41] and Rotor-Gene-Q (Qiagen), using a modified protocol [42,43]. PpMC1 has 2 cysteines: C10 and C209. The CPM stocks (5 mg mL^{-1} in DMSO) were diluted to 0.1 mg mL^{-1} and equilibrated with purification buffer B for 10 min in the dark, before mixing with 12 μg purified protein and 10 mM compound (5 mM for NAD^+) to a final volume of 50 μL. When required, inhibitors were added to a final concentration of 10 μM. The mixture was equilibrated for a further 10 min in the dark at 4 °C. The fluorescent intensity was measured at 460 nm (excitation) and 510 nm (emission) from 25 °C to 90 °C with a ramp of 1 °C every 15 s. Data analysis and determination of the apparent melting temperature (Tm) of the protein were carried out with the software provided with the instrument. ΔTm was calculated by subtracting the apparent melting temperature of protein without compound from the apparent melting temperature in the presence of compound: a positive ΔTm suggests the compound binds protein.

2.7. Protein reconstitution into liposomes

A mix containing *E. coli* polar lipid extract, egg L-α-phosphatidylcholine and tetraoleoyl cardiolipin (all from Avanti Polar Lipids) in a 15:5:1 (w/w) ratio was dried under a stream of nitrogen. The lipids were rehydrated in 20 mM HEPES pH 7.0 and 50 mM NaCl. The detergent pentaethylene glycol monodecyl ether ($C_{10}E_5$) was added to a final concentration of 2.5% (v/v) and the lipids were solubilised by vortexing and incubated on ice: the equivalent of 30 μg protein was added per sample. The pentaethylene glycol monodecyl was removed by SM-2 bio-beads (Bio-Rad): five additions of bio-beads were made to the master mix every 20 min with inversion at 4 °C: four of 30 mg, and the final of 240 mg per sample. The samples were incubated overnight at 4 °C with rolling. Bio-beads were removed by passage through empty micro-bio spin columns (Bio-Rad). Compound, to a final concentration of 5 mM, was internalized by freeze-thaw-extrusion [39]. When required, inhibitors were added to a final concentration of 10 μM. The sample was subjected to three cycles of freeze-thawing in liquid nitrogen for 2 min, followed by thawing in a room temperature water bath for 10 min. The proteoliposomes were subsequently extruded by 21 passages through a 0.4-μm filter (Millipore) [39]. The external substrate was removed and exchanged into buffer (20 mM HEPES, pH 7.0 and 50 mM NaCl) using a PD10 desalting column (GE Healthcare).

2.8. Transport assays

Transport assays were performed using the Hamilton MicroLab Star robot (Hamilton Robotics Ltd). The proteoliposomes (100 μL) were loaded into the wells of a MultiScreenHTS + HA 96-well filter plate (pore size 0.45-μm, Millipore). Uptake of radiolabel was initiated by the addition of 100 μL buffer containing 5 μM [^{33}P]-ATP (Hartmann Analytic). Uptake was stopped after 0, 10, 20, 30, 45, 60, 150, 300, 450 and 600 s by filtration and washing thrice with 200 μL ice-cold buffer (20 mM HEPES, pH 7.0, 50 mM NaCl). For Km analysis, 1 mM ATP was internalized by freeze-thaw-extrusion. Eight concentrations of [^{33}P]-ATP were prepared, and uptake of radiolabel was initiated by the

addition of 100 μL buffer containing: 0.5 μM (5 GBq mmol^{-1}), 1 μM (5 GBq mmol^{-1}), 2.5 μM (5 GBq mmol^{-1}), 5 μM (5 GBq mmol^{-1}), 10 μM (1 GBq mmol^{-1}), 25 μM (1 GBq mmol^{-1}), 50 μM (1 GBq mmol^{-1}) and 100 μM (1 GBq mmol^{-1}). Uptake was stopped after 0, 10, 20, 30, 40, 50, 60, 90, and 150 s by filtration and washing. The plates were dried overnight, 200 μL MicroScint-20 (PerkinElmer) was added, and levels of radioactivity were determined using a TopCount scintillation counter (PerkinElmer). The initial rates were determined from the linear part of the uptake curve (60 s).

2.9. SDS-PAGE analysis and protein quantification

Protein was visualised by SDS-PAGE analysis using 4–12% bis-tris mPAGE gels (Merck) according to the manufacturer's instructions and stained using InstantBlue (Abcam). The reconstitution efficiency was determined by comparing the amount of protein incorporated into proteoliposomes with a standard curve of known amounts of purified protein.

3. Results

3.1. Mitochondrial carriers of Paratrimastix pyriformis

We built a phylogenetic tree containing the four known *P. pyriformis* carriers and human and yeast SLC25 proteins to provide a basis for substrate specificity prediction (Fig. S1). The analysis showed that *P. pyriformis* mitochondrial carriers 2–4 clustered with human NAD, folate/FAD, and outer membrane carriers, respectively. *P. pyriformis* mitochondrial carrier 1 (PpMC1, UniProt accession code: B0F463) grouped in the clan of thiamine pyrophosphate (TPP), AAC, APC, and coenzyme A (CoA) carriers. As none of the enzymes present in the MRO of *P. pyriformis* require TPP or CoA [30] (Fig. 1), it is unlikely that PpMC1 transports these cofactors. Hence, we considered PpMC1 as the most likely candidate for an adenine nucleotide carrier.

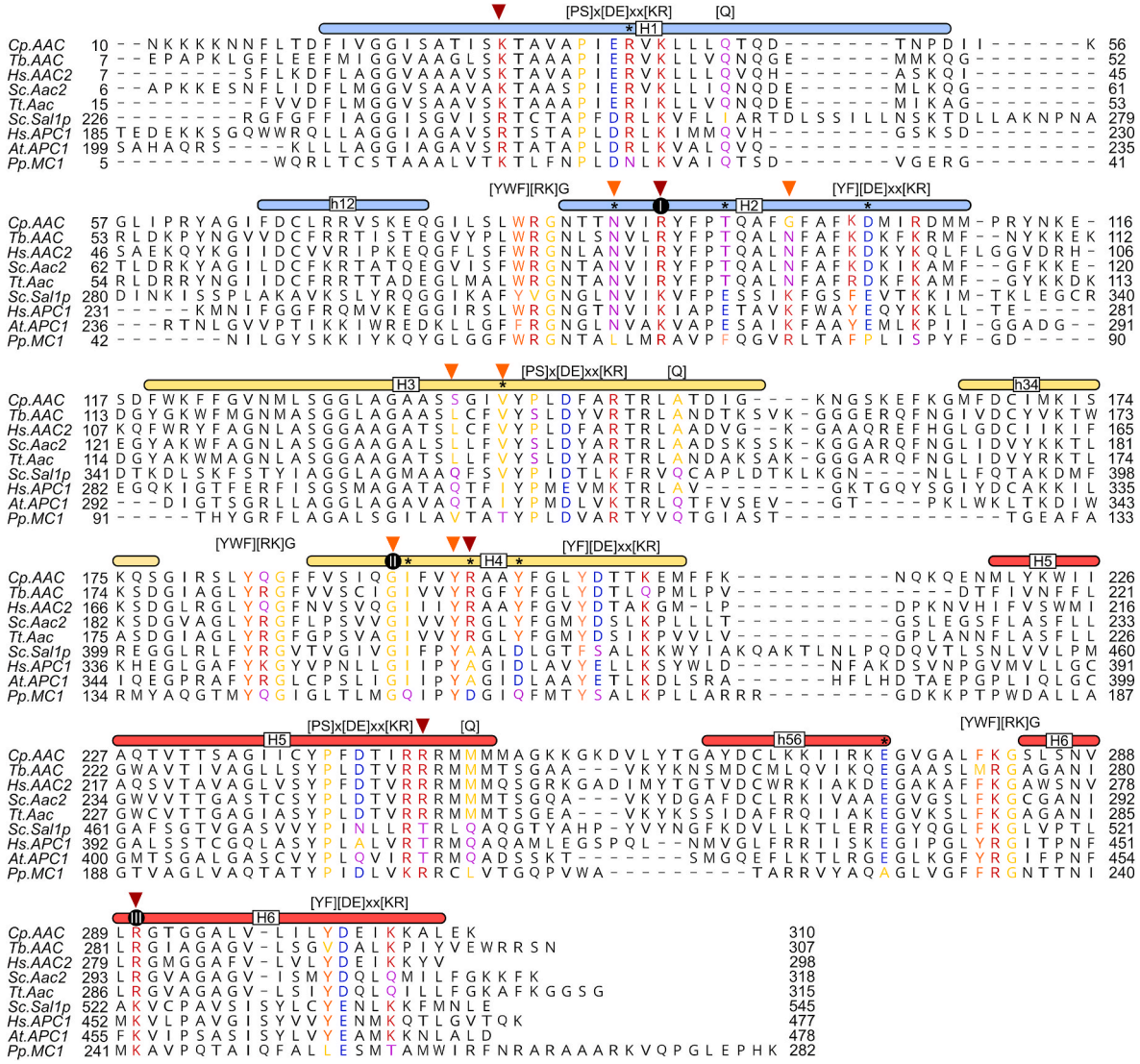

Fig. 2. Alignment of PpMC1 with selected AAC and APC carriers.
Repeats 1, 2 and 3 that contain odd-numbered transmembrane α-helix (H1, H3, H5), matrix α-helix (h12, h34, h56), and even-numbered transmembrane α-helix (H2, H4, H6) are coloured blue, yellow and red, respectively. Cardiolipin binding sites [YWF][RK]G, matrix salt-bridge network [PS]x[DE]xx[KR], glutamine braces [Q], cytosolic salt-bridge network [YF][DE]xx[KR] are highlighted. The contact points of substrate binding sites are shown in black circles. Red triangles indicate the positively charged amino acids interacting with phosphate groups of ADP/ATP and orange triangles are highlighting residues interacting with adenine ring of transported substrates. The peculiar features of PpMC1 are highlighted by asterisk symbol. Amino acids are coloured according to their properties: acidic D, E are blue; basic K, R, H are red; polar C, N, Q, S, T are magenta; aliphatic P, G, A, I, L, M, V are yellow; aromatic F, Y, W are orange. Cp, *Cryptosporidium parvum*; Tb, *Trypanosoma brucei*; Hs, *Homo sapiens*; Sc, *Saccharomyces cerevisiae*; Tt, *Thermothelomyces thermophila;* At, *Arabidopsis thaliana*; Pp, *Paratrimastix pyriformis.*

3.2. Sequence analysis of the putative adenine nucleotide carrier of Paratrimastix pyriformis

To reveal whether PpMC1 possesses features of adenine nucleotide carriers, we compared its sequence with experimentally confirmed AAC proteins [6,13,17,44,45] and the carrier domain of APC [22,24,46] from different organisms. The key features common to all members of the SLC25 protein family, namely cardiolipin binding sites [9,12], matrix [9,11,12] and cytosolic salt bridge networks [10,12,13,15,47], glutamine [12] and tyrosine braces [15], and proline kinks [9,12] are conserved in PpMC1 (Fig. 2, Fig. 3a). The three contact points (I-III) located in the centre of the cavity are the main interaction sites [47,48]. The residues of contact point II distinguish between the classes of transported substrates: the typical residue for nucleotide transporters at contact point II is a G residue, followed by an aliphatic residue [IVLM]. Contact point I discriminates within substrates of the same class, and contact point III usually exhibits a positively charged amino acid [47,49]. PpMC1 has the same residues in all three contact points as AAC and APC (positively charged residues in I and III and a glycine residue in II). The only noticeable difference is a glutamine residue, next to glycine in contact point II, instead of the typical aliphatic residue [IVLM] (Fig. 2).

AAC and APC share similar substrate binding sites [14,21,47] that involve other residues in addition to the three contact points [12,14,15,47,48]. Five positively charged amino acids at positions K30, R88 (contact point I), R197, R246, R287 in *Thermothelomyces thermophila* AAC (TtAac) have been demonstrated to be crucial for carrier function and proposed to interact with negatively charged phosphate groups of the substrate [12,48], four of which are conserved in PpMC1 (K19, K71, R207, K242) (Fig. 2, red triangles). The exception is the third positively charged residue, which is aspartic acid (D156) in PpMC1. Other important residues thought to be relevant for interaction with the adenine moiety are N85, N96, L135, V138, G192 (contact point II), and Y196 in TtAac [48]. PpMC1 exhibits mostly similar amino acids in the three key positions (V107, G151, Y155) (Fig. 2, orange triangles). In case of the APC, two negatively charged residues (E264/D361 in human APC1, E318/D424 in yeast Sal1p) were proposed to be binding sites for

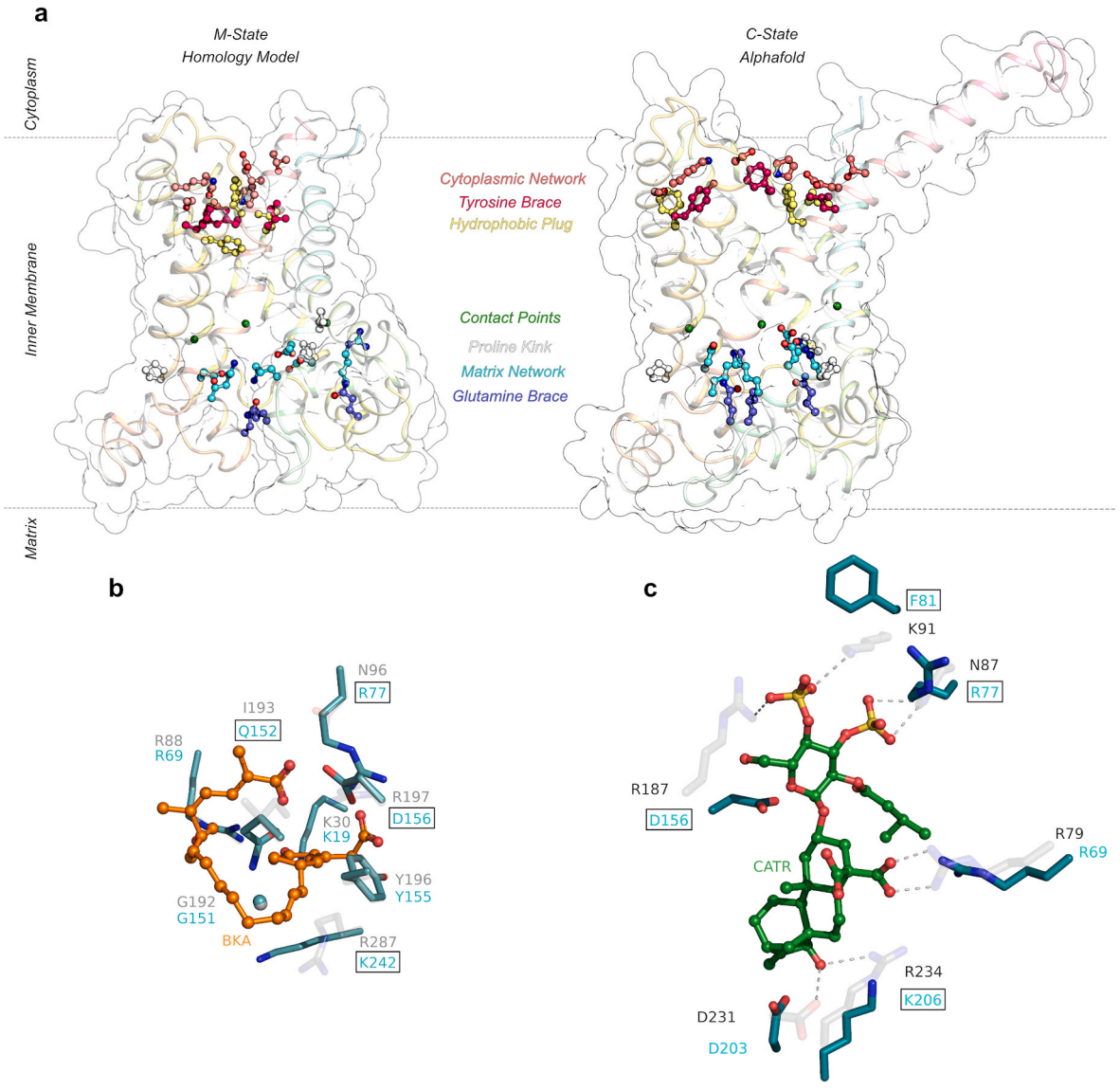

Fig. 3. PpMC1 has all of the key features of a functional ADP/ATP, but lacks residues involved in CATR and BKA binding. **a)** Structural models of PpMC1, in the matrix-open state (left), based on TtAac (Protein Data Bank entry; 6GCI), and cytoplasmic-open state (right), predicted from AlphaFold. The residues of the cytoplasmic network (orange), tyrosine-brace (red), hydrophobic plug (yellow), pro-kink (grey), matrix network (cyan), contact points (green) and glutamine-brace (blue) are indicated. Residues and interactions involved in **b)** BKA (TtAac, 6GCI) and **c)** CATR (BtAAC, 1OKC) binding are shown in light grey with interactions as light grey dashed lines; equivalent residues in PpMC1 are shown in colour.

Mg^{2+} [14,21,47]. These residues are not conserved in AAC [14,21,47], and are also absent in PpMC1. A comparison of the sequence of PpMC1 with AAC and APC indicates that this carrier may transport adenine nucleotides, although exhibiting some divergent features (Fig. 2, highlighted with an asterisk).

To reveal whether the amino acids responsible for the interaction with CATR and BKA are conserved, we compared a model of PpMC1 with the structure of TtAac in complex with BKA [15] (Fig. 3b), and with the ADP/ATP carrier of *Bos taurus* (BtAAC) in complex with CATR [9] (Fig. 3c). Most amino acids involved in the interaction with CATR or BKA are not conserved in PpMC1, hence rendering their binding to the carrier unlikely.

3.3. Screening of potential PpMC1 substrates by thermostability shift assay

To screen potential substrates of PpMC1, we first expressed the protein in *Saccharomyces cerevisiae* [38] and purified it in the detergent dodecyl maltose neopentyl glycol (Fig. 4a). A protein of about 60 kDa co-purified with PpMC1 (32 kDa), confirmed by mass spectrometry to be the yeast chaperone Hsp60, a common contaminant observed in carrier purifications. Next, we used thermostability analysis to evaluate its protein stability. As the protein unfolds in a temperature ramp, previously inaccessible cysteines become available to react with the thiol-specific probe CPM, leading to an increase in fluorescence [41,42]. This assay produces an apparent melting temperature (Tm), which represents the temperature at which approximately half the protein population is unfolded in a homogeneous sample. PpMC1 indeed produced an unfolding curve, confirming that the protein is folded (Fig. 4b). The apparent melting temperature for PpMC1 (Tm = 50.7 ± 0.3 °C) is similar to the Tm of other mitochondrial ADP/ATP carrier proteins (human AAC1, apparent Tm = 47.0 ± 1 °C [39]; *T. thermophila* Aac, apparent Tm = 50.2 ± 0.6 °C [13,48]; *S. cerevisiae* Aac2, apparent Tm = 44.7 ± 0.3 °C [42]).

It has been previously shown that both inhibitors [39,42,50] and substrates [40,48] of transport proteins can specifically stabilise proteins in thermal denaturation assays, thus providing a simple and high-throughput tool for screening libraries of potential binders. We constructed a library of 15 compounds, which included nucleotides, inorganic ions, and the canonical AAC inhibitors CATR and BKA and screened it against detergent-solubilised, purified protein. To quantify the effect of a compound, a temperature shift (ΔTm) was calculated, which is the difference in apparent melting temperature in the presence and absence of compound. A positive ΔTm suggests that the protein is stabilised by the compound because of binding, generating substrate candidate. Among the tested compounds only ATP (ΔTm = 8.7 ± 0.1 °C), ADP (ΔTm = 12.2 ± 0.8 °C), CATR (ΔTm = 4.3 ± 0.2 °C) and TTP (ΔTm = 3.4 ± 0.1 °C), stabilised the protein by more than 3 °C (Fig. 4c).

3.4. Substrate specificity and kinetics of PpMC1

To test whether a particular compound is transported, we loaded proteoliposomes with 5 mM substrate by freeze-thaw-extrusion [39] and initialized exchange by the addition of 5 μM radiolabeled [^{33}P]-ATP on the outside. Only when the internalized compound is a transportable substrate of the carrier will uptake of radiolabel occur. Uptake was observed for ATP (19.1 ± 2.8 nmol [^{33}P]-ATP mg^{-1} min^{-1}), ADP (18.6 ± 1.2 nmol [^{33}P]-ATP mg^{-1} min^{-1}), and, to a lesser extent, AMP (8.3 ± 3.9 nmol [^{33}P]-ATP mg^{-1} min^{-1}) (Fig. 4d and **e**). GTP, TTP, and phosphate were not transported by PpMC1 (Fig. 4e). As expected, neither CATR nor BKA inhibited uptake of [^{33}P]-ATP (Fig. 4e), given the lack of conservation in their binding sites (Fig. 3b and c). We also determined the apparent K_m of the transport, which is the concentration of substrate at half maximal rate (Fig. 4f and **g**). The K_m of PpMC1 was 38 μM (95% confidence interval = 28–53 μM), an order of magnitude higher than the K_m observed of the human AAC1 (3.2 μM) [39], but comparable to the K_m of human APC1 (31 μM) [21].

3.5. Phylogenetic analysis of PpMC1 protein

To elucidate the relationship of PpMC1 with AAC and APC, we built a dataset of 141 sequences: 82 AAC, 44 APC with and without calmodulin-like regulatory domain [18,25], 13 sequences of SLC25 proteins from metamonads (including the carrier of *T. gallinae* [26]) and the previously described distinct ADP/ATP carriers from *E. histolytica* [27] and *A. locustae* [7]. As expected, AAC and APC orthologues formed separate groups and none of the transporters from parasitic protists previously described as distinct ADP/ATP carriers clustered with them (Fig. 5, Fig. S2), but formed two groupings closer to APC in the unrooted tree. The long branch of PpMC1 indicates that the sequence of this protein is divergent even within its clan. The phylogenetic position of the carriers from previously described parasitic protists, as well as PpMC1, revealed that these carriers are distinct from canonical AAC and APC, thus may represent a distinct class (es) of adenine nucleotide carriers.

4. Discussion

In this study, we have functionally and phylogenetically characterised one of the four carriers from the modified mitochondrion of the free-living protist *P. pyriformis*. Phylogenetic analysis and sequence comparison of PpMC1 with AAC and APC indicated its potential role in nucleotide transport. Of the 15 compounds tested in thermostability shift analyses, only ATP and ADP caused a noticeable shift of apparent melting temperature indicating that they bound to PpMC1 (Fig. 4b and **c**). Interestingly, the addition of CATR also resulted in an increase in protein stability of 4.3 ± 0.2 °C, but the stabilisation is much smaller than observed for mitochondrial ADP/ATP carriers (HsAAC1, ΔTm = 33.0 °C [39]; TtAac, ΔTm = 33.0 °C [13]; ScAac2, ΔTm = 27.5 °C [42]). BKA, the other canonical inhibitor of archetypal AAC, did not lead to a significant stabilisation to the protein (ΔTm = 0.4 ± 0.1 °C). The results of the thermostability shift assay are consistent with altered inhibitor binding sites revealed by the sequence alignment of PpMC1 with AAC and APC proteins (Fig. 2) as well as the comparison of the PpMC1 model with structure of BtAAC and TtAac (Fig. 3b and **c**).

The transport assay with proteoliposomes demonstrated that PpMC1 exhibits similar biochemical properties to the previously described ADP/ATP carriers of *E. histolytica* [27,28], *A. locustae* [7] and *T. gallinae* [26]. The substrate specificity of PpMC1 is limited to ATP, ADP, and, to a lesser extent AMP, as observed for the SLC25 protein of *A. locustae*. The substrate specificity of *E. histolytica* carrier was shown to be broader (ATP, ADP, AMP, PAPS), while the *T. gallinae* hydrogenosomal protein 31 (TgHMP31) transported only ATP and ADP. The K_m of PpMC1 (38 μM) was comparable to the K_m of the mitosomal carrier of *A. locustae* (31.2 μM) [7] and 3.5-fold lower than the K_m of the *T. gallinae* carrier (134.2 μM) [26]. In comparison to HsAAC1 (Km = 3.2 μM), PpMC1 has a 10-fold lower affinity to ATP and instead resembles the affinity of the APC to ATP [22,23]. Furthermore, PpMC1, as with the three previously characterised parasitic protist carriers, is insensitive to the canonical AAC inhibitors. Finally, it was proposed that the carrier present in *E. histolytica* mitosomes, in a similar fashion to APC, mediated electroneutral exchange of substrates that did not depend on membrane potential, since the transport assay was not affected by valinomycin [22,27]. Despite the number of commonalities with APC, none of these carriers are capable of phosphate transport (Fig. 4c and **e**), lack the conserved negatively charged residues considered to interact with Mg^{2+}, and do not possess the additional calmodulin-like regulatory domain typical of APC.

The three previously characterised carriers of parasitic protists were described as distinct ADP/ATP carriers based not only on biochemical properties, but also their phylogenetic origin. None of them clustered amongst AAC carriers in the phylogenetic tree, and the *A. locustae* carrier

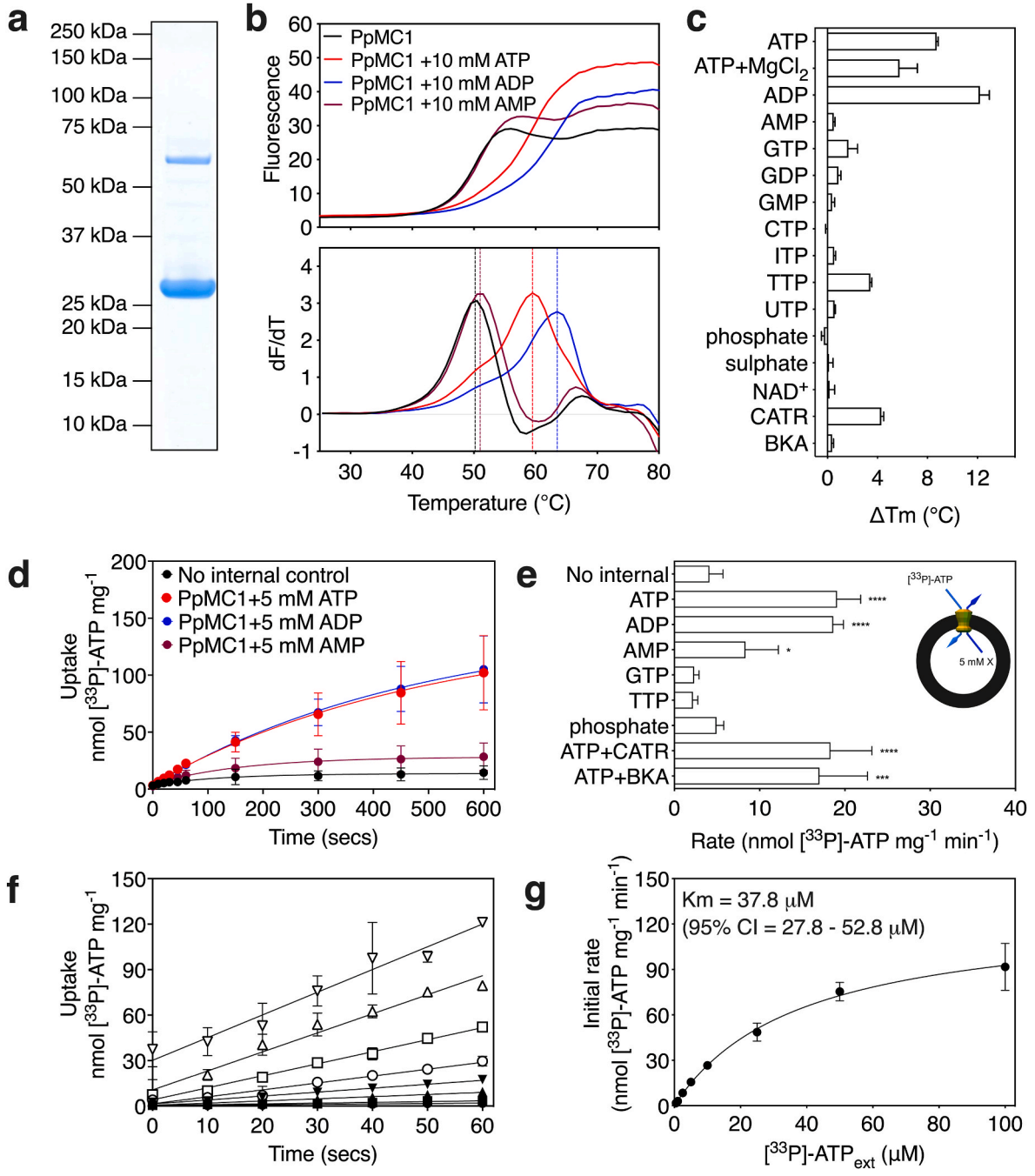

Fig. 4. Expression, purification, and biophysical characterization of PpMC1. **a**) Instant-blue stained SDS-PAGE gel of purified PpMC1. The contaminant (at approximately 60 kDa) is Hsp60 (identified by mass spectrometry). **b**) Typical unfolding curves of 12 μg PpMC1 without compound (black trace), PpMC1+10 mM ATP (red trace), PpMC1+10 mM ADP (blue trace) and PpMC1+10 mM AMP (maroon trace). The peak in the derivative of the unfolding curve (dF/dT) is the apparent melting temperature (Tm). **c**) Thermostability screening of PpMC1 against 10 mM compound (5 mM for NAD^+, 10 μM for CATR and BKA). The temperature shift (ΔTm) is the apparent melting temperature in the presence of compound minus the apparent melting temperature in the absence of compound. The data are represented by the mean and standard deviation of at least three biological repeats. **d**) [^{33}P]-ATP uptake curves of PpMC1 reconstituted into proteoliposomes loaded without substrate (black circles), 5 mM ATP (red trace), 5 mM ADP (blue trace) or 5 mM AMP (maroon trace). Transport was initiated by the external addition of 5 μM [^{33}P]-ATP. **e**) Proteoliposomes were loaded with 5 mM substrate by freeze-thaw-extrusion. Where indicated, inhibitors were added to a final concentration of 10 μM. Initial transport rates were calculated from the linear part of the uptake curve (60 s). The data represent the mean and standard deviation of three biological repeats, each the average of two technical repeats. Student's t-tests assuming unequal variances were performed for the significance analysis (0.05<p-value: not significant; 0.01<p-value<0.05: *; 0.001<p-value<0.01: **; 0.0001<p-value<0.001: ***; p-value<0.0001: ****). **f**) Proteoliposomes containing PpMC1 were loaded with 1 mM ATP, and transport initiated by the addition of externally added [^{33}P]-ATP at either 0.5 (black circles), 1.0 (black squares), 2.5 (black up triangles), 5.0 (black down triangles), 10 (open circles), 25 (open squares), 50 (open up triangles) or 100 (open down triangles) μM. The initial rate was calculated over the linear part of the uptake curve (60 s) by linear regression. The data represent the average and standard deviation of three technical repeats. **g**) Kinetics of [^{33}P]-ATP uptake. The apparent Km was determined using the Michaelis-Menten function in Prism (GraphPad). The data represent the mean and standard deviation of three technical repeats.

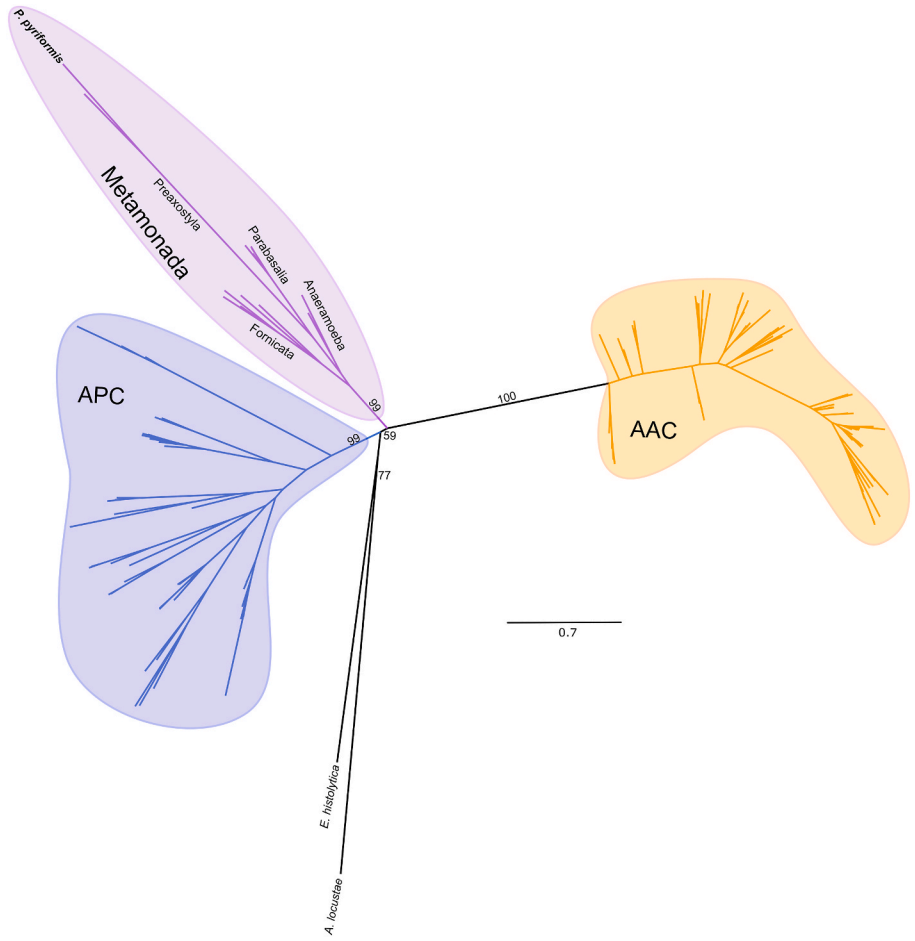

Fig. 5. Phylogenetic analysis of adenine nucleotide carriers.
The maximum likelihood tree was generated by IQ-TREE with the LG+F+R7 model suggested by ModelFinder. Tree support was calculated using ultrafast bootstrap analysis. The support values are shown only for main branches.

was placed within the group of NAD and FAD/folate transporters [7,26,27]. To corroborate the position of these distinct ADP/ATP carriers using a richer dataset available today, we built a tree with APC and AAC proteins from different groups of eukaryotes. As in the recent study by Catalan et al. (2021) [18], orthologs of these two types of carriers formed separate groups, suggesting their independent origin (Fig. 4, Fig. S2). ADP/ATP carriers are more widespread, present in most eukaryotes with a few exceptions [18,19,51,52] and are clearly distinct from APC. PpMC1, TgHMP31 and the putative adenine nucleotide carriers from other metamonads, as well as the carriers from *E. histolytica* and *A. locustae,* cluster neither within the AAC or the APC groups, but formed two branches in the vicinity of APC. Given the functional and structural differences from APC, it is likely these carriers represent a distinct class or classes of adenine nucleotide carriers from both AAC and APC.

The lower affinity to ATP of PpMC1, TgHMP31 and the carrier of *A. locustae* than HsAAC1 may indicate that the production and export of ATP is not the primary role of MROs present in these organisms. In aerobic mitochondria, AAC mediate the extremely high ADP and ATP transport rates required for oxidative phosphorylation, which in humans is estimated to be equivalent to our own body weight every day [53]. On the other hand, ATP is not produced in mitosomes, and therefore it needs to be imported into the organelle to supply its metabolism and to power import of proteins [2]. The MRO of *P. pyriformis* requires ATP to activate lipoic acid (cofactor of the H protein of the glycine cleavage system) and for polyglutamylation of folate species to maintain its pool in the organelle (Fig. 1) [30]. At the same time, the MRO is capable of producing ATP in the reaction resulting in formate production [30]. Therefore, the PpMC1 characterised in this study is likely used to balance the adenine nucleotide pool of the organelle and the cell.

Author contributions

Conceptualization, V·H and E.R.S·K.; methodology, M.S·K., E.R.S·K., and V·H.; investigation, J.Z., M.S·K., E.P., P·P.D. and A.C·K; validation, J. Z and M.S·K; formal analysis, J.Z. and M.S·K.; resources, V·H and E.R.S·K.; data curation, J. Z, E.P and M.S·K.; writing—original draft preparation, J. Z, M.S·K., V·H and P·P.D.; writing—review and editing, J.Z., M.S·K., P·P.D., E.P., A.C·K., V.H. and E.R.S·K.; visualization, J.Z., M.S·K., A.C·K.; V·H., and E.R.S·K.; supervision, V.H. and E.R.S·K.; project administration, M.S·K.; V.H. and E.R.S·K.; funding acquisition, V·H., J. Z and E.R.S.K. All authors have read and agreed to the published version of the manuscript.

Funding

This work was supported by the European Research Council (ERC) under the European Union's Horizon 2020 research and innovation programme [grant agreement No 771592] to V·H., P·P.D. and J.Z.; Grant Agency of Charles University [Project No. 1162320] to J.Z. and V·H.; grant from the Ministry of Education, Youth and Sports (MEYS) of the Czech Republic (CR) in the Centre for research of pathogenicity and virulence of parasites [project No. CZ.02.1.01/0.0/0.0/16_019/0000759] to V·H.; Medical Research Council [grant MC_UU_00028/

2UK] to M.S·K., A.C·K., and E.R.S·K., The Research Council of Norway [grant 301170] to E.P.

Data availability

Alignments used to construct phylogenetic trees have been deposited and are publicly available as of the date of publication at FigShare: DOI 10.6084/m9.figshare.22317793. Any additional information required to reanalyse the data reported in this paper is available from the lead contact upon request.

Declaration of competing interest

The authors declare that they have no known competing financial interests or personal relationships that could have appeared to influence the work reported in this paper.

Appendix A. Supplementary data

Supplementary data to this article can be found online at https://doi.org/10.1016/j.abb.2023.109638.

References

[1] E.R.S. Kunji, A. Aleksandrova, M.S. King, H. Majd, V.L. Ashton, E. Cerson, R. Springett, M. Kibalchenko, S. Tavoulari, P.G. Crichton, J.J. Ruprecht, The transport mechanism of the mitochondrial ADP/ATP carrier, Biochim. Biophys. Acta 1863 (2016) 2379–2393, https://doi.org/10.1016/J.BBAMCR.2016.03.015.

[2] K. Hjort, A.V. Goldberg, A.D. Tsaousis, R.P. Hirt, T.M. Embley, Diversity and reductive evolution of mitochondria among microbial eukaryotes, Philos. Trans. R. Soc. Lond. B Biol. Sci. 365 (2010) 713–727, https://doi.org/10.1098/RSTB.2009.0224.

[3] P.J. Kang, J. Ostermann, J. Shilling, W. Neupert, E.A. Craig, N. Pfanner, Requirement for hsp70 in the mitochondrial matrix for translocation and folding of precursor proteins, Nature 348 (1990) 137–143, https://doi.org/10.1038/348137a0.

[4] J.J. Ruprecht, E.R.S. Kunji, The SLC25 mitochondrial carrier family: structure and mechanism, Trends Biochem. Sci. 45 (2020) 244–258, https://doi.org/10.1016/J.TIBS.2019.11.001.

[5] F. Palmieri, M. Monné, Discoveries, metabolic roles and diseases of mitochondrial carriers: a review, Biochim. Biophys. Acta 1863 (2016) 2362–2378, https://doi.org/10.1016/J.BBAMCR.2016.03.007.

[6] M.S. King, S. Tavoulari, V. Mavridou, A.C. King, J. Mifsud, E.R.S. Kunji, A single cysteine residue in the translocation pathway of the mitosomal ADP/ATP carrier from *Cryptosporidium parvum* confers a broad nucleotide specificity, Int. J. Mol. Sci. 21 (2020) 8971, https://doi.org/10.3390/IJMS21238971.

[7] B.A.P. Williams, I. Haferkamp, P.J. Keeling, An ADP/ATP-Specific mitochondrial carrier protein in the microsporidian *Antonospora locustae*, J. Mol. Biol. 375 (2008) 1249–1257, https://doi.org/10.1016/J.JMB.2007.11.005.

[8] M. Saraste, J.E. Walker, Internal sequence repeats and the path of polypeptide in mitochondrial ADP/ATP translocase, FEBS Lett. 144 (1982) 250–254, https://doi.org/10.1016/0014-5793(82)80648-0.

[9] E. Pebay-Peyroula, C. Dahout-Gonzalez, R. Kahn, V. Trézéguet, G.J.M. Lauquin, G. Brandolin, Structure of mitochondrial ADP/ATP carrier in complex with carboxyatractyloside, Nature 426 (2003) 39–44, https://doi.org/10.1038/nature02056.

[10] J.J. Ruprecht, E.R. Kunji, Structural changes in the transport cycle of the mitochondrial ADP/ATP carrier, Curr. Opin. Struct. Biol. 57 (2019) 135–144, https://doi.org/10.1016/J.SBI.2019.03.029.

[11] D.R. Nelson, C.M. Felix, J.M. Swanson, Highly conserved charge-pair networks in the mitochondrial carrier family, J. Mol. Biol. 277 (1998) 285–308, https://doi.org/10.1006/JMBI.1997.1594.

[12] J.J. Ruprecht, A.M. Hellawell, M. Harding, P.G. Crichton, A.J. McCoy, E.R.S. Kunji, Structures of yeast mitochondrial ADP/ATP carriers support a domain-based alternating-access transport mechanism, Proc. Natl. Acad. Sci. U. S. A. 111 (2014) E426–E434, https://doi.org/10.1073/PNAS.1320692111/SUPPL_FILE/SAPP.PDF.

[13] M.S. King, M. Kerr, P.G. Crichton, R. Springett, E.R.S. Kunji, Formation of a cytoplasmic salt bridge network in the matrix state is a fundamental step in the transport mechanism of the mitochondrial ADP/ATP carrier, Biochim. Biophys. Acta 1857 (2016) 14–22, https://doi.org/10.1016/J.BBABIO.2015.09.013.

[14] A.J. Robinson, C. Overy, E.R.S. Kunji, The mechanism of transport by mitochondrial carriers based on analysis of symmetry, Proc. Natl. Acad. Sci. U. S. A. 105 (2008) 17766–17771, https://doi.org/10.1073/PNAS.0809580105/SUPPL_FILE/APPENDIX_PDF.PDF.

[15] J.J. Ruprecht, M.S. King, T. Zögg, A.A. Aleksandrova, E. Pardon, P.G. Crichton, J. Steyaert, E.R.S. Kunji, The molecular mechanism of transport by the mitochondrial ADP/ATP carrier, Cell 176 (2019) 435–447.e15, https://doi.org/10.1016/j.cell.2018.11.025.

[16] E. Pfaff, M. Klingenberg, Adenine nucleotide translocation of mitochondria, Eur. J. Biochem. 6 (1968) 66–79, https://doi.org/10.1111/J.1432-1033.1968.TB00420.X.

[17] J. Mifsud, S. Ravaud, E.M. Krammer, C. Chipot, E.R.S. Kunji, E. Pebay-Peyroula, F. Dehez, The substrate specificity of the human ADP/ATP carrier AAC1, Mol. Membr. Biol. 30 (2013) 160–168, https://doi.org/10.3109/09687688.2012.745175.

[18] S. García-Catalán, L. González-Moreno, A. del Arco, Ca2+-regulated mitochondrial carriers of ATP-Mg2+/Pi: evolutionary insights in protozoans, Biochim. Biophys. Acta Mol. Cell Res. 1868 (2021), 119038, https://doi.org/10.1016/J.BBAMCR.2021.119038.

[19] M. van der Giezen, D.J. Slotboom, D.S. Horner, P.L. Dyal, M. Harding, G.P. Xue, T. M. Embley, E.R.S. Kunji, Conserved properties of hydrogenosomal and mitochondrial ADP/ATP carriers: a common origin for both organelles, EMBO J. 21 (2002) 572–579, https://doi.org/10.1093/EMBOJ/21.4.572.

[20] S.P.D. Harborne, M.S. King, P.G. Crichton, E.R.S. Kunji, Calcium regulation of the human mitochondrial ATP-Mg/Pi carrier SLC25A24 uses a locking pin mechanism, Sci. Rep. 7 (2017) 1–13, https://doi.org/10.1038/srep45383.

[21] S.P.D. Harborne, E.R.S. Kunji, Calcium-regulated mitochondrial ATP-Mg/Pi carriers evolved from a fusion of an EF-hand regulatory domain with a mitochondrial ADP/ATP carrier-like domain, IUBMB Life 70 (2018) 1222–1232, https://doi.org/10.1002/IUB.1931.

[22] G. Fiermonte, F. de Leonardis, S. Todisco, L. Palmieri, F.M. Lasorsa, F. Palmieri, Identification of the mitochondrial ATP-Mg/Pi transporter. Bacterial expression, reconstitution, functional characterization, and tissue distribution, J. Biol. Chem. 279 (2004) 30722–30730, https://doi.org/10.1074/JBC.M400445200.

[23] M. Monné, D.V. Miniero, T. Obata, L. Daddabbo, L. Palmieri, A. Vozza, M. C. Nicolardi, A.R. Fernie, F. Palmieri, Functional characterization and organ distribution of three mitochondrial ATP-Mg/Pi carriers in *Arabidopsis thaliana*, Biochim. Biophys. Acta 1847 (2015) 1220–1230, https://doi.org/10.1016/J.BBABIO.2015.06.015.

[24] J. Traba, E.M. Froschauer, G. Wiesenberger, J. Satrústegui, A. del Arco, Yeast mitochondria import ATP through the calcium-dependent ATP-Mg/Pi carrier Sal1p, and are ATP consumers during aerobic growth in glucose, Mol. Microbiol. 69 (2008) 570–585, https://doi.org/10.1111/J.1365-2958.2008.06300.X.

[25] J. Traba, J. Satrústegui, A. del Arco, Characterization of SCaMC-3-like/slc25a41, a novel calcium-independent mitochondrial ATP-Mg/Pi carrier, Biochem. J. 418 (2009) 125–133, https://doi.org/10.1042/BJ20081262.

[26] J. Tjaden, I. Haferkamp, B. Boxma, A.G.M. Tielens, M. Huynen, J.H.P. Hackstein, A divergent ADP/ATP carrier in the hydrogenosomes of *Trichomonas gallinae* argues for an independent origin of these organelles, Mol. Microbiol. 51 (2004) 1439–1446, https://doi.org/10.1111/J.1365-2958.2004.03918.X.

[27] K.W. Chan, D.J. Slotboom, S. Cox, T.M. Embley, O. Fabre, M. van der Giezen, M. Harding, D.S. Horner, E.R.S. Kunji, G. León-Avila, J. Tovar, A novel ADP/ATP transporter in the mitosome of the microaerophilic human parasite *Entamoeba histolytica*, Curr. Biol. 15 (2005) 737–742, https://doi.org/10.1016/j.cub.2005.02.068.

[28] F. Mi-Ichi, A. Nozawa, H. Yoshida, Y. Tozawa, T. Nozaki, Evidence that the *Entamoeba histolytica* mitochondrial carrier family links mitosomal and cytosolic pathways through exchange of 3'-phosphoadenosine 5'-phosphosulfate and ATP, Eukaryot. Cell 14 (2015) 1144–1150, https://doi.org/10.1128/EC.00130-15/ASSET/0138F990-6D11-439C-8111-D71B19D46776/ASSETS/GRAPHIC/ZEK9990944930005.JPEG.

[29] V. Hampl, L. Hug, J.W. Leigh, J.B. Dacks, B.F. Lang, A.G.B. Simpson, A.J. Roger, Phylogenomic analyses support the monophyly of Excavata and resolve relationships among eukaryotic "supergroups,", Proc. Natl. Acad. Sci. U. S. A. 106 (2009) 3859–3864, https://doi.org/10.1073/PNAS.0807880106/SUPPL_FILE/0807880106SI.PDF.

[30] J. Zítek, Z. Füssy, S.C. Treitli, P. Peña-Diaz, Z. Vaitová, D. Zavadska, K. Harant, V. Hampl, Reduced mitochondria provide an essential function for the cytosolic methionine cycle, Curr. Biol. 32 (2022) 5057–5068, https://doi.org/10.1016/J.CUB.2022.10.028.

[31] J.J. Braymer, S.A. Freibert, M. Rakwalska-Bange, R. Lill, Mechanistic concepts of iron-sulfur protein biogenesis in Biology, Biochim. Biophys. Acta Mol. Cell Res. 1868 (2021), 118863, https://doi.org/10.1016/J.BBAMCR.2020.118863.

[32] Z. Zubáčová, L. Novák, J. Bublíková, V. Vacek, J. Fousek, J. Rídl, J. Tachezy, P. Doležal, Č. Vlček, V. Hampl, The mitochondrion-like organelle of *Trimastix pyriformis* contains the complete Glycine cleavage system, PLoS One 8 (2013), e55417, https://doi.org/10.1371/JOURNAL.PONE.0055417.

[33] J. Jumper, R. Evans, A. Pritzel, T. Green, M. Figurnov, O. Ronneberger, K. Tunyasuvunakool, R. Bates, A. Žídek, A. Potapenko, A. Bridgland, C. Meyer, S.A. A. Kohl, A.J. Ballard, A. Cowie, B. Romera-Paredes, S. Nikolov, R. Jain, J. Adler, T. Back, S. Petersen, D. Reiman, E. Clancy, M. Zielinski, M. Steinegger, M. Pacholska, T. Berghammer, S. Bodenstein, D. Silver, O. Vinyals, A.W. Senior, K. Kavukcuoglu, P. Kohli, D. Hassabis, Highly accurate protein structure prediction with AlphaFold, Nature 596 (2021) 7873, https://doi.org/10.1038/s41586-021-03819-2, 596 (2021) 583–589.

[34] A. Waterhouse, M. Bertoni, S. Bienert, G. Studer, G. Tauriello, R. Gumienny, F. T. Heer, T.A.P. De Beer, C. Rempfer, L. Bordoli, R. Lepore, T. Schwede, SWISS-MODEL: homology modelling of protein structures and complexes, Nucleic Acids Res. 46 (2018) W296, https://doi.org/10.1093/NAR/GKY427. –W303.

[35] K. Katoh, D.M. Standley, MAFFT multiple sequence alignment software version 7: improvements in performance and usability, Mol. Biol. Evol. 30 (2013) 772–780, https://doi.org/10.1093/MOLBEV/MST010.

[36] A. Criscuolo, S. Gribaldo, BMGE (Block Mapping and Gathering with Entropy): a new software for selection of phylogenetic informative regions from multiple

sequence alignments, BMC Evol. Biol. 10 (2010) 1–21, https://doi.org/10.1186/1471-2148-10-210/FIGURES/9.
[37] L.T. Nguyen, H.A. Schmidt, A. von Haeseler, B.Q. Minh, IQ-TREE: a fast and effective stochastic algorithm for estimating maximum-likelihood phylogenies, Mol. Biol. Evol. 32 (2015) 268–274, https://doi.org/10.1093/MOLBEV/MSU300.
[38] M.S. King, E.R.S. Kunji, Expression and purification of membrane proteins in *Saccharomyces cerevisiae*, Methods Mol. Biol. 2127 (2020) 47–61, https://doi.org/10.1007/978-1-0716-0373-4_4/COVER.
[39] S. Jaiquel Baron, M.S. King, E.R.S. Kunji, T.J.J. Schirris, Characterization of drug-induced human mitochondrial ADP/ATP carrier inhibition, Theranostics 11 (2021) 5077–5091, https://doi.org/10.7150/THNO.54936.
[40] H. Majd, M.S. King, S.M. Palmer, A.C. Smith, L.D.H. Elbourne, I.T. Paulsen, D. Sharples, P.J.F. Henderson, E.R.S. Kunji, Screening of candidate substrates and coupling ions of transporters by thermostability shift assays, Elife 7 (2018), 38821, https://doi.org/10.7554/ELIFE.38821.
[41] A.I. Alexandrov, M. Mileni, E.Y.T. Chien, M.A. Hanson, R.C. Stevens, Microscale fluorescent thermal stability assay for membrane proteins, Structure 16 (2008) 351–359, https://doi.org/10.1016/j.str.2008.02.004.
[42] P.G. Crichton, Y. Lee, J.J. Ruprecht, E. Cerson, C. Thangaratnarajah, M.S. King, E. R.S. Kunji, Trends in thermostability provide information on the nature of substrate, inhibitor, and lipid interactions with mitochondrial carriers, J. Biol. Chem. 290 (2015) 8206–8217, https://doi.org/10.1074/jbc.M114.616607.
[43] S.P.D. Harborne, M.S. King, E.R.S. Kunji, Thermostability assays: a generic and versatile tool for studying the functional and structural properties of membrane proteins in detergents, Methods Mol. Biol. 2168 (2020) 105–121, https://doi.org/10.1007/978-1-0716-0724-4_5/COVER.
[44] P. Peña-Diaz, L. Pelosi, C. Ebikeme, C. Colasante, F. Gao, F. Bringaud, F. Voncken, Functional characterization of TbMCP5, a conserved and essential ADP/ATP carrier present in the mitochondrion of the human pathogen trypanosoma brucei, J. Biol. Chem. 287 (2012), 41861, https://doi.org/10.1074/JBC.M112.404699.
[45] M. Monné, K.W. Chan, D.-J. Slotboom, E.R.S. Kunji, Functional expression of eukaryotic membrane proteins in *Lactococcus lactis*, Protein Sci. 14 (2005) 3048, https://doi.org/10.1110/PS.051689905.
[46] A. Lorenz, M. Lorenz, U.C. Vothknecht, S. Niopek-Witz, H.E. Neuhaus, I. Haferkamp, *In vitro* analyses of mitochondrial ATP/phosphate carriers from *Arabidopsis thaliana* revealed unexpected Ca2+-effects, BMC Plant Biol. 15 (2015), https://doi.org/10.1186/S12870-015-0616-0.
[47] A.J. Robinson, E.R.S. Kunji, Mitochondrial carriers in the cytoplasmic state have a common substrate binding site, Proc. Natl. Acad. Sci. U. S. A. 103 (2006) 2617–2622, https://doi.org/10.1073/PNAS.0509994103/SUPPL_FILE/09994TABLE3.PDF.
[48] V. Mavridou, M.S. King, S. Tavoulari, J.J. Ruprecht, S.M. Palmer, E.R.S. Kunji, Substrate binding in the mitochondrial ADP/ATP carrier is a step-wise process guiding the structural changes in the transport cycle, Nat. Commun. 13 (2022) 3585, https://doi.org/10.1038/s41467-022-31366-5.
[49] E.R.S. Kunji, A.J. Robinson, The conserved substrate binding site of mitochondrial carriers, Biochim. Biophys. Acta 1757 (2006) 1237–1248, https://doi.org/10.1016/J.BBABIO.2006.03.021.
[50] S. Tavoulari, T.J.J. Schirris, V. Mavridou, C. Thangaratnarajah, M.S. King, D.T. D. Jones, S. Ding, I.M. Fearnley, E.R.S. Kunji, Key features of inhibitor binding to the human mitochondrial pyruvate carrier hetero-dimer, Mol. Metabol. 60 (2022), 101469, https://doi.org/10.1016/J.MOLMET.2022.101469.
[51] P.L. Jedelský, P. Doležal, P. Rada, J. Pyrih, O. Šmíd, I. Hrdý, M. Šedinová, M. Marcinčíková, L. Voleman, A.J. Perry, N.C. Beltrán, T. Lithgow, J. Tachezy, The minimal proteome in the reduced mitochondrion of the parasitic protist *Giardia intestinalis*, PLoS One 6 (2011), e17285, https://doi.org/10.1371/JOURNAL.PONE.0017285.
[52] Z. Füssy, M. Vinopalová, S.C. Treitli, T. Pánek, P. Smejkalová, I. Čepička, P. Doležal, V. Hampl, Retortamonads from vertebrate hosts share features of anaerobic metabolism and pre-adaptations to parasitism with diplomonads, Parasitol. Int. 82 (2021), 102308, https://doi.org/10.1016/J.PARINT.2021.102308.
[53] M.J. Buono, F.W. Kolkhorst, Estimating ATP resynthesis during a marathon run: a method to introduce metabolism, Adv. Physiol. Educ. 25 (2001) 70–71, https://doi.org/10.1152/ADVANCES.2001.25.2.70.